Non-locality of the Willis coupling in fluid laminates

Matthieu Malléjac, Théo Cavalieri, Vicente Romero-García, Aurélien Merkel, Daniel Torrent, Johan Christensen, Jensen Li, Jean-Philippe Groby

Non-locality of the Willis coupling in fluid laminates

Matthieu Malléjac, Théo Cavalieri, V. Romero-García

Laboratoire d'Acoustique de l'Université du Mans (LAUM), UMR 6613, Institut d'Acoustique - Graduate School (IA-GS), CNRS, Le Mans Université, France.

Aurélien Merkel

Université de Lorraine, CNRS, IJL, F-54000 Nancy, France.

Daniel Torrent

GROC, UJI, Institut de Noves Tecnologies de la Imatge (INIT), Universitat Jaume I, 12071 Castelló, Spain.

Johan Christensen

Department of Physics, Universidad Carlos III de Madrid, Leganés, Madrid, Spain.

Jensen Li

Department of Physics, The Hong Kong University of Science and Technology, Clear Water Bay, Hong Kong, China.

Jean-Philippe Groby*

Laboratoire d'Acoustique de l'Université du Mans (LAUM), UMR 6613, Institut d'Acoustique - Graduate School (IA-GS), CNRS, Le Mans Université, France.

Abstract

The closed form expressions of the effective properties in periodic fluid laminates are derived thanks to the Padé approximation of the transfer matrix. A second-order Taylor expansion of the transfer matrix elements exhibits Willis coupling. This coupling is the sum of a local term and a nonlocal term. The nonlocal term arises from the apparent bulk modulus in quasi one-dimensional problems. The nonlocality directly impacts the governing equations modeling the acoustic wave propagation in these Willis materials, which then involve convolution products in space. As an example, a two-orthotropic porous material laminate

*Corresponding author
Email address: Jean-Philippe.Groby@univ-lemans.fr (Jean-Philippe Groby)

is considered. The theoretically derived effective properties and scattering coefficients are found in excellent agreement with those numerically calculated. The Willis coupling widens the frequency range of validity and accuracy of the effective properties and thus of the calculated scattering coefficients when compared to classical homogenization results for which the Willis coupling is absent. This widening mostly relies on the effect of Willis coupling on the impedance of the fluid laminate. The effective properties are finally derived for a general laminate.

Keywords: Willis coupling, Non-locality, Laminate structures

2010 MSC: 00-01, 99-00

---

1. Introduction

Since the seminal work of Willis in the 80's [1], the eponymous materials have received an increasing attention, because of their analogy with bi-isotropic electromagnetic metamaterials [2]. The Willis coupling parameters couple the potential and kinetic energies in the acoustic conservation relations, therefore enhancing the ability to control waves in asymmetric [3, 4, 5, 6, 7, 8, 9, 10] or non-reciprocal [11, 12, 13, 14, 15] systems. Willis couplings effectively appear along the diagonal of the propagation matrix, i.e., the Hamiltonian, either with opposite signs to account for the structural asymmetry, i.e., the even coupling, or with identical signs to account for the non-reciprocity and/or non-locality, i.e., the odd coupling [6]. Non-locality arises from spatial dispersion and translates into the dependence of the effective properties on the wavenumber [16]. In acoustics, only a few articles tackled the problem of non-locality [17, 18, 19, 20, 21]. In order to investigate the nonlocal Willis coupling, we consider a simple asymmetric fluid laminate excited at oblique incidence, thus extending results derived at normal incidence notably in [22]. The effective properties are derived by considering the Padé approximation of the transfer matrix that relates the state vectors at both sides of the unit cell. A second-order Taylor expansion is required to derive effective density tensor, bulk modulus,

and Willis coupling. Similar results were derived in electromagnetism in [23] using the Baker–Campbell–Hausdorff formula [24]. Laminate fluid-like porous structures are often used to achieve impedance matching for absorption or insulation purposes [25, 26, 27]. As an example, we thus consider a two-orthotropic fluid-like porous material laminate.

The article is organized as follows. The propagation matrix of a general Willis material layer is derived in Subsection 2.1. The formulation to evaluate the effective properties in reciprocal structures is reminded in Subsection 2.2 and applied to a two-material unit cell fluid laminate in Section 3. In Section 4, the apparent and effective properties as well as the scattering coefficients of a two-orthotropic fluid-like porous material laminate are discussed. Finally, the general forms of the effective properties are derived for a general anisotropic fluid laminate in Section 5.

2. General statement

2.1. Wave propagation in a planar Willis medium

Assuming an implicit time dependence $\mathrm{e}^{-\mathrm{i}\omega t}$ and locality of the medium, i.e., the intrinsic medium parameters are independent of the spatial coordinate $\mathbf{x}$, the pressure p and velocity $\mathbf{V}$ satisfy the following equations in a general Willis fluid medium

$$\begin{aligned} \mathrm{i}\omega\bar{\boldsymbol{\xi}}p + \mathrm{i}\omega\bar{\bar{\boldsymbol{\rho}}}\cdot\mathbf{V} &= \nabla p, \\ \mathrm{i}\omega\bar{\boldsymbol{\zeta}}\cdot\mathbf{V} + \mathrm{i}\omega C p &= \nabla\cdot\mathbf{V}, \end{aligned} \tag{1}$$

where $\bar{\boldsymbol{\xi}}$ and $\bar{\boldsymbol{\zeta}}$ are Willis couplings, $\bar{\bar{\boldsymbol{\rho}}}$ is the mass density tensor, and C is the compressibility, which is inverse to the bulk modulus $B = 1/C$. We consider a layer of such material, invariant in the plane $\mathbf{x}_\perp = (\mathbf{x}_1, \mathbf{x}_2)$ and of thickness L along the x_3-direction, as sketched in Fig. 1 (a). The Cartesian coordinate system attached to the layer is assumed to match the principal directions of the material such that $\bar{\bar{\boldsymbol{\rho}}} = \mathbf{diag}\,(\rho_j)$, $j = 1, 2, 3$. The spatial Fourier transform of Eq. (1) can thus be cast in the form

$$\frac{\partial}{\partial x_3}\mathbf{W} = \mathbf{A}\cdot\mathbf{W}, \tag{2}$$

where $\mathbf{W} =< \tilde{p}, \tilde{V}_3 >^T$ is the state vector formed by the spatial Fourier transforms $\tilde{p}$ and $\tilde{V}_3$ of p and $\mathbf{V} \cdot \mathbf{x}_3 = V_3$ respectively and $\mathbf{A}$ is the propagation matrix that reads as

$$\mathbf{A} = \mathrm{i}\omega \begin{bmatrix} \xi_3 & \rho_3 \\ C - \dfrac{(k_1 - \omega\zeta_1)(k_1 - \omega\xi_1)}{\omega^2\rho_1} - \dfrac{(k_2 - \omega\zeta_2)(k_2 - \omega\xi_2)}{\omega^2\rho_2} & \zeta_3 \end{bmatrix}. \tag{3}$$

The details of the derivation are provided in Appendix A. Note that each element of the propagation matrix is that along the $\mathbf{x_3}$ direction, but that related to the compressibility, i.e., the a_{21} component. This element accounts for both the propagation direction in the plane $\mathbf{x}_\perp$ via its dependence on the in-plane wavenumber components $\mathbf{k}_\perp =< k_1, k_2 >$ and the properties of the material along these in-plane directions. This element is usually cast in the form of an apparent compressibility [28, 29]

$$\begin{aligned} C_a &= C - \frac{(k_1 - \omega\zeta_1)(k_1 - \omega\xi_1)}{\omega^2\rho_1} - \frac{(k_2 - \omega\zeta_2)(k_2 - \omega\xi_2)}{\omega^2\rho_2} \\ &= C - \frac{k_1^2}{\omega^2\rho_1} - \frac{k_2^2}{\omega^2\rho_2} + \frac{k_1\omega(\zeta_1 + \xi_1)}{\omega^2\rho_1} + \frac{k_2\omega(\zeta_2 + \xi_2)}{\omega^2\rho_2} - \frac{\zeta_1\xi_1}{\rho_1} - \frac{\zeta_2\xi_2}{\rho_2}, \end{aligned} \tag{4}$$

while the material is obviously local. Therefore, this type of system is often described as quasi one-dimensional, because its propagation matrix is formally written as that of a one-dimensional system [30, 28, 29]. The solution to Eq. (2) relates the state vector at $x_3 = L$ to that at $x_3 = 0$ via the matrix exponential, i.e., the transfer matrix, $\mathbf{W}(l) = \mathbf{exp}(\mathbf{A}l)\,\mathbf{W}(0) = \mathbf{T}_l\mathbf{W}(0)$.

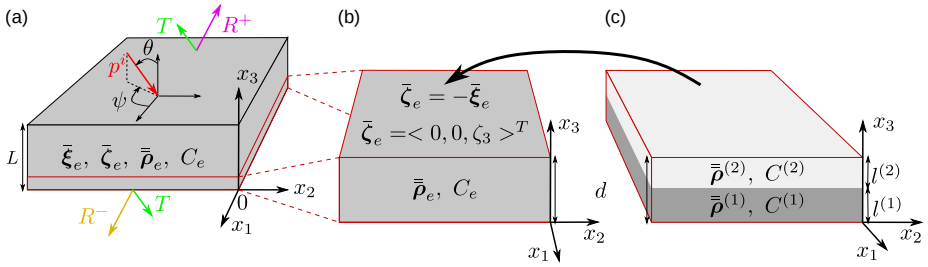

Figure 1: [Color online] Sketch of a L-thich layer of a general Willis fluid (a), of the d-thick unit cell of the Willis fluid, and of the two-orthotropic fluid laminate unit cell (c).

2.2. Calculation of the effective properties from the knowledge of the unit cell transfer matrix

We assume a quasi one-dimensional reciprocal and asymmetric system composed of a d-periodic unit cell of respective propagation matrix $\mathbf{A^e}$. The state vectors at both sides of the unit cell, $\mathbf{W}(d)$ and $\mathbf{W}(0)$, are related to each other through the 2×2 transfer matrix $\mathbf{T}_d = \mathbf{exp}\left(\mathbf{A^e}d\right)$ of elements t_{ij}, $(i,j) \in [1,2]^2$. Following Ref. [22], the propagation matrix is correctly approximated by the inversion of the first-order Padé approximation of the matrix exponential,

$$\begin{aligned}\mathbf{A^e} &\approx \frac{2}{d}(\mathbf{T}_d + \mathbf{I})^{-1}(\mathbf{T}_d - \mathbf{I}) \\ &\approx \frac{2}{d}\frac{1}{2 + t_{11} + t_{22}} \begin{bmatrix} t_{11} - t_{22} & 2t_{12} \\ 2t_{21} & t_{22} - t_{11} \end{bmatrix},\end{aligned} \tag{5}$$

where the reciprocity of the system has been accounted for by imposing $\det\left(\mathbf{T}_d\right) = 1$ and $\mathbf{I}$ is the identity matrix. This form directly provides the apparent elements of the propagation matrix of a quasi one-dimensional Willis material, Eq. (3), from which the Willis parameters and the other effective properties can be efficiently calculated, as sketched in Fig. 1 (b). The effective parameters derived following this procedure are indicated by a superscript e in the following.

3. Effective properties of the reciprocal laminated two-material unit-cell structure

We consider a laminated unit cell of thickness d composed of a layer of material $M^{(1)}$ of density tensor $\bar{\bar{\boldsymbol{\rho}}}^{(1)}$, compressiblity $C^{(1)}$, and thickness $l^{(1)}$, and a layer of material $M^{(2)}$ of density tensor $\bar{\bar{\boldsymbol{\rho}}}^{(2)}$, compressiblity $C^{(2)}$, and thickness $l^{(2)} = d - l^{(1)}$, as sketched in Fig. 1 (c). The state vectors at both sides of the unit cell are thus related by the total transfer matrix composed of the multiplication of the transfer matrices modeling the propagation in each layer

$$\mathbf{W}(d) = \mathbf{T}_d\mathbf{W}(0) = \mathbf{T}_{l^{(2)}}\mathbf{T}_{l^{(1)}}\mathbf{W}(0), \tag{6}$$

where $\mathbf{T}_{l^{(j)}} = \mathbf{exp}\left(\mathbf{A}^{(j)} l^{(j)}\right)$, $j = 1, 2$, is the transfer matrix of the layer of material $M^{(j)}$ over the thickness $l^{(j)}$, with $\mathbf{A}^{(j)}$ the propagation matrix of each anisotropic layer of the laminate simply obtained when the Willis couplings in Eq. (3) vanish, i.e., $\bar{\boldsymbol{\xi}} = \bar{\boldsymbol{\zeta}} = \mathbf{0}$ [28]. These transfer matrices read as

$$\mathbf{T}_{l^{(j)}} = \begin{bmatrix} \cos\left(k_a^{(j)} l^{(j)}\right) & \mathrm{i} Z_a^{(j)} \sin\left(k_a^{(j)} l^{(j)}\right) \\ \dfrac{\mathrm{i}}{Z_a^{(j)}} \sin\left(k_a^{(j)} l^{(j)}\right) & \cos\left(k_a^{(j)} l^{(j)}\right) \end{bmatrix}, \tag{7}$$

where $k_a^{(j)} = \omega\sqrt{C_a^{(j)} \rho_3^{(j)}}$ is nothing but the projection of the wavenumber along the $\mathbf{x}_3$-axis, i.e., $k_a^{(j)} = k_3^{(j)}$, and $Z_a^{(j)} = \sqrt{\rho_3^{(j)} / C_a^{(j)}}$, $j = 1, 2$. Assuming $\lambda \gg d$ in such a way that $k_a^{(1)} l^{(1)}$ and $k_a^{(2)} l^{(2)}$ are much smaller than 1 and making use of Eq. (5) leads to the following propagation matrix components a_{ij}^e, $(i, j) \in [1, 2]^2$

$$\begin{aligned} a_{11}^e = -a_{22}^e &= \frac{\omega^2 l^{(1)} l^{(2)}}{2d} \left(C_a^{(2)} \rho_3^{(1)} - C_a^{(1)} \rho_3^{(2)} \right) \\ &= \frac{\omega^2 l^{(1)} l^{(2)}}{2d} \left(C^{(2)} \rho_3^{(1)} - C^{(1)} \rho_3^{(2)} + \frac{(k_1)^2}{\omega^2} \left(\frac{\rho_3^{(2)}}{\rho_1^{(1)}} - \frac{\rho_3^{(1)}}{\rho_1^{(2)}} \right) + \frac{(k_2)^2}{\omega^2} \left(\frac{\rho_3^{(2)}}{\rho_2^{(1)}} - \frac{\rho_3^{(1)}}{\rho_2^{(2)}} \right) \right) , \\ a_{12}^e &= \mathrm{i}\omega \frac{\rho_3^{(1)} l^{(1)} + \rho_3^{(2)} l^{(2)}}{d} , \\ a_{21}^e &= \mathrm{i}\omega \frac{C_a^{(1)} l^{(1)} + C_a^{(2)} l^{(2)}}{d} \\ &= \mathrm{i}\omega \frac{C^{(1)} l^{(1)} + C^{(2)} l^{(2)}}{d} - \frac{\mathrm{i}}{\omega} \left(\frac{l^{(1)}}{d\rho_1^{(1)}} + \frac{l^{(2)}}{d\rho_1^{(2)}} \right) (k_1)^2 - \frac{\mathrm{i}}{\omega} \left(\frac{l^{(1)}}{d\rho_2^{(1)}} + \frac{l^{(2)}}{d\rho_2^{(2)}} \right) (k_2)^2 . \end{aligned} \tag{8}$$

The details of the calculation are provided in Appendix B. Note that these expressions are identical to those derived via the Baker–Campbell–Hausdorff formula in Appendix C. By identifying Eq. (8) with Eq. (3), we obtain on the one hand

$$\rho_3^e = \frac{\rho_3^{(1)} l^{(1)} + \rho_3^{(2)} l^{(2)}}{d}, \ \frac{1}{\rho_1^e} = \frac{l^{(1)}}{d\rho_1^{(1)}} + \frac{l^{(2)}}{d\rho_1^{(2)}}, \ \frac{1}{\rho_2^e} = \frac{l^{(1)}}{d\rho_2^{(1)}} + \frac{l^{(2)}}{d\rho_2^{(2)}} , \qquad C^e = \frac{C^{(1)} l^{(1)} + C^{(2)} l^{(2)}}{d} , \tag{9}$$

which are classical results from the homogenization theory, when first-order Taylor expansion is considered, i.e., $\mathcal{O}\left((kd)^2\right)$, and on the other hand

$$\xi_1^e = -\zeta_1^e = 0,\ \xi_2^e = -\zeta_2^e = 0,$$
$$\zeta_3^e = -\xi_3^e = \frac{-\mathrm{i}\omega l^{(1)} l^{(2)}}{2d}\left(C^{(2)}\rho_3^{(1)} - C^{(1)}\rho_3^{(2)} + \frac{(k_1)^2}{\omega^2}\left(\frac{\rho_3^{(2)}}{\rho_1^{(1)}} - \frac{\rho_3^{(1)}}{\rho_1^{(2)}}\right) + \frac{(k_2)^2}{\omega^2}\left(\frac{\rho_3^{(2)}}{\rho_2^{(1)}} - \frac{\rho_3^{(1)}}{\rho_2^{(2)}}\right)\right), \tag{10}$$

when second-order Taylor expansion is considered, i.e., $\mathcal{O}\left((kd)^3\right)$. This last result applies several comments.

First, the structure being symmetric along the $\mathbf{x_1}$ and $\mathbf{x_2}$ directions, the results $\xi_1^e = -\zeta_1^e = 0$ and $\xi_2^e = -\zeta_2^e = 0$ were expected. Nevertheless, this result must be tempered by analyzing Eq. (4) in terms of power of ω. Assuming ζ_j and ξ_j, $j = 1, 2$, of $\mathcal{O}\left(\omega^2\right)$ as it is usually the case for reciprocal Willis material [6, 22], the last two terms of Eq. (4) are $\mathcal{O}\left(\omega^3\right)$, which would imply a third-order Taylor expansion of the transfer matrix elements, i.e., $\mathcal{O}\left((kd)^4\right)$. Rigorously, we can only conclude that $\xi_1^e = -\zeta_1^e$ and $\xi_2^e = -\zeta_2^e$ in the absence of analysis of the current system, i.e., by noticing that the structure is symmetric along the $\mathbf{x_1}$ and $\mathbf{x_2}$ directions. In the general case, the propagation of a plane wave along each principal direction, i.e., along the directions x_1, x_2, and x_3 must be successively considered. This induces a permutation of the indices in the propagation matrix, thus allowing a direct determination of the remaining Willis coupling elements which are then located along the diagonal of the propagation matrix. Nevertheless, this point should be moderated, because all elements of the propagation matrix are $O\left(kd\right)^3$. Thus, these two last terms could be avoided because they are $O\left(kd\right)^4$. The Willis couplings along these directions are $\mathcal{O}\left(\omega^2\right)$ as the other, except the last two terms of the propagation matrix should not impact the scattering coefficients, because they become of higher order.

Second, the structure being reciprocal, we have $\boldsymbol{\xi}^e = -\boldsymbol{\zeta}^e$.

Third, the even Willis coupling ζ_3^e is the sum of a local term, i.e., $\frac{-\mathrm{i}\omega l^{(1)} l^{(2)}}{2d}\left(C^{(2)}\rho_3^{(1)} - C^{(1)}\rho_3^{(2)}\right)$, and of a nonlocal term, i.e., $\frac{-\mathrm{i}\omega l^{(1)} l^{(2)}}{2d}\left(\frac{(k_1)^2}{\omega^2}\left(\frac{\rho_3^{(2)}}{\rho_1^{(1)}} - \frac{\rho_3^{(1)}}{\rho_1^{(2)}}\right) + \frac{(k_2)^2}{\omega^2}\left(\frac{\rho_3^{(2)}}{\rho_2^{(1)}} - \frac{\rho_3^{(1)}}{\rho_2^{(2)}}\right)\right)$. Note that the local term is that derived in Ref. [22]. The initial form of the

whole Willis coupling is that of the local term where the compressibilities are the apparent compressibilities, i.e., $C_a^{(j)}$, $j = 1, 2$. The non-locality thus arises from the dependence of the apparent compressibilities on $\mathbf{k}_\perp = (\mathbf{k}_1, \mathbf{k}_2)$. Nevertheless, this non-locality is effective and not apparent.

Fourth, the nonlocal Willis coupling is even in that formulation and not odd as proposed in Ref. [6]. Nevertheless, both Willis couplings, i.e., the local and the nonlocal couplings, are the difference of properties between the material $M^{(1)}$ and $M^{(2)}$, while all the other effective properties are weighted sums of both material properties. The x_3-direction of propagation is thus implicit and is accounted for when solving the bounded system. This was already pointed out in Ref. [6], where the odd feature is attributed to the phase change over the unit cell, which will change sign with the opposite propagation direction.

Fifth, the Willis coupling is a linear function of the frequency in the absence of dispersion. While the first-order Taylor expansion gives rise to constitutive equations that are characteristic of symmetric structures, i.e., classical homogenization with $\mathbf{A}^H =< [0\ \mathrm{i}\omega\rho_3^e], [\mathrm{i}\omega C_a^e\ 0] >^T$, the second-order Taylor expansion reveals Willis coupling that is characteristic of asymmetric structures. In the quasi-static limit, an asymmetric laminated structure generally falls back to a symmetric structure.

All these remarks suggest that the governing equations in a Willis material composed of a fluid laminate unit cell should rather be of the form

$$\begin{aligned} -\mathrm{i}\omega\bar{\boldsymbol{\zeta}} \star_\perp p + \mathrm{i}\omega\bar{\bar{\boldsymbol{\rho}}} \cdot \mathbf{V} &= \nabla p, \\ \mathrm{i}\omega\bar{\boldsymbol{\zeta}} \star_\perp \cdot\mathbf{V} + \mathrm{i}\omega C p &= \nabla \cdot \mathbf{V}, \end{aligned} \tag{11}$$

where $\star_\perp$ expresses the convolution product in the in-plane space, as detailed in Appendix D. This last system highlights the dependence of the Willis coupling on the in-plane coordinates and thus the non-locality features. Nevertheless, this dependence does not take the usual form of non-locality, which would rather be on the whole Cartesian coordinates and in particular on the x_3-coordinate. It is more closely related to a dependence of the Willis coupling on the angle of

incidence and thus suggests that the form of the governing equations, although providing the accurate propagation matrix, could be inadequate to describe the three-dimensional acoustic wave propagation in fluid laminates. This is also in accordance with the fact that this non-locality only relies on the dependence of the apparent compressibility on $\mathbf{k}_\perp$.

4. Results and discussion

We consider a fluid-like laminated structure composed of two air-saturated porous materials as depicted in Fig. 2 (a). Both materials consist in the periodic repetition of the micro-structure unit-cell sketched in the inset of Fig. 2 (a). This micro-structure unit-cell is generated by extruding an ellipsoid from a cuboid, the semi-axes of which are longer than the associated cuboid sides [28]. This assumption is fundamental to form an open porosity material. The respective micro-structure unit cells of the two materials $M^{(1)}$ and $M^{(2)}$ differ in the cuboid and ellipsoid dimensions. The skeletons are assumed motionless. The resulting equivalent fluids are orthotropic because the ellipsoid is centered in the cuboid and the in-plane dimensions are imposed as identical. Each material is thus fully characterized by the porosity ϕ, the thermal characteristic length Λ', the thermal permeability Θ, the in-plane and out-of-plane tortuosities $\alpha_\perp = \alpha_1 = \alpha_2$ and $\alpha_\parallel = \alpha_3$, the in-plane and out-of-plane viscous characteristic lengths $\Lambda_\perp$ and $\Lambda_\parallel$, and the in-plane and out-of-plane viscous permeabilities $K_\perp$ and $K_\parallel$. These porous material properties are scaled by the thicknesses $l_c^{(1)} = 300$ μm and $l_c^{(2)} = 75$ μm of the $M^{(1)}$ and $M^{(2)}$ material micro-structures and are calculated with a two-scale homogenization procedure [27, 28, 31]. They are listed in Table 1. The complex and frequency dependent effective densities and bulk modulus take the forms [32, 33]

$$\begin{aligned}
\frac{\rho_h}{\rho_0} &= \frac{\alpha_h}{\phi} + \mathrm{i}\,\frac{\eta/K_h}{\omega\rho_0}\sqrt{1-\frac{\mathrm{i}\omega\rho_0}{\eta}\left(\frac{2\alpha_h K_h}{\phi\Lambda_h}\right)^2},\ h=\parallel,\perp\ , \\
\frac{B_0}{B} &= \phi\left(\gamma+(\gamma-1)\left(1+\mathrm{i}\,\frac{\phi\eta/\Theta}{\omega\mathrm{Pr}\rho_0}\sqrt{1-\frac{\mathrm{i}\omega\mathrm{Pr}\rho_0}{\eta}\left(\frac{2\Theta}{\phi\Lambda'}\right)^2}\right)^{-1}\right)\ ,
\end{aligned} \tag{12}$$

	$M^{(1)}$	$M^{(2)}$
l_c (μm)	300	75
ϕ	0.6718	0.6718
Λ' (m)	$0.8637 \times l_c^{(1)}$	$0.8906 \times l_c^{(2)}$
Θ (mm^2)	$0.08545 \times \left(l_c^{(1)}\right)^2$	$0.1220 \times \left(l_c^{(2)}\right)^2$
$\alpha_\perp$	1.3572	1.3486
$\alpha_\parallel$	2.8903	3.1570
$\Lambda_\perp$ (μm)	$0.5713 \times l_c^{(1)}$	$0.6030 \times l_c^{(2)}$
$\Lambda_\parallel$ (μm)	$0.7599 \times l_c^{(1)}$	$1.00175 \times l_c^{(2)}$
$K_\perp$ (mm^2)	$0.01612 \times \left(l_c^{(1)}\right)^2$	$0.01766 \times \left(l_c^{(2)}\right)^2$
$K_\parallel$ (mm^2)	$0.03568 \times \left(l_c^{(1)}\right)^2$	$0.06464 \times \left(l_c^{(2)}\right)^2$

Table 1: Acoustic properties of the fluid-like porous materials.

where the air density is $\rho_0 = 1.213$ kg.m^{-3}, the adiabatic constant is $\gamma = 1.4$, the dynamic viscosity is $\eta = 1.839 \times 10^{-5}$ Pa.s, the Prandtl number is Pr $= 0.71$, and the air bulk modulus is $B_0 = \gamma P_0$, with the atmospheric pressure $P_0 = 1.013 \times 10^5$ Pa.

The layer thicknesses are $l^{(1)} = 2$ cm and $l^{(2)} = 1$ cm, such that $d = l^{(1)} + l^{(2)} = 3$ cm. The effective and apparent properties as calculated from Eqs. (8, 9), and (10) are compared to those as numerically calculated from $\mathbf{log}\left(\mathbf{T}_L\right) = \mathbf{A}^e_{num} L$. The structure is $L = Nd$-thick, $N \in \mathbb{N}$, i.e., an integer number of repetition of the unit cell, and is excited by a plane incident wave initially propagating in the air medium that surrounds the laminate, with θ and ψ the elevation and azimutal angles such that $k_1 = k_0 \sin(\theta)\cos(\psi)$, $k_2 = k_0 \sin(\theta)\sin(\psi)$, and $k_3^{(0)} = k_0 \cos(\theta)$, as shown in Fig. 1 (a). The scattering coefficients are the reflection coefficients R^+, when the structure is excited from the x_3 positive axis, and R^-, when the structure is excited from the x_3 negative axis, and the transmission coefficient T. These scattering coefficients

are calculated from the transfer matrix via

$$\begin{aligned} R^+ &= \frac{t_{11} - t_{12}/\bar{Z}_0 + \bar{Z}_0 t_{21} - t_{22}}{t_{11} - t_{12}/\bar{Z}_0 - \bar{Z}_0 t_{21} + t_{22}},\ R^- = \frac{-t_{11} - t_{12}/\bar{Z}_0 + \bar{Z}_0 t_{21} + t_{22}}{t_{11} - t_{12}/\bar{Z}_0 - \bar{Z}_0 t_{21} + t_{22}}, \\ T &= \frac{2}{t_{11} - t_{12}/\bar{Z}_0 - \bar{Z}_0 t_{21} + t_{22}}, \end{aligned} \tag{13}$$

where $\bar{Z}_0 = Z_0/\cos(\theta)$ is the reduced impedance that accounts for the elevation angle, with the air impedance $Z_0 = \sqrt{B_0\rho_0}$. The transfer matrix elements used in Eq. (13) are either those of $\mathbf{T}_L$ or those of $\mathbf{T}_L^e = \mathbf{exp}(\mathbf{A}^e L)$. Note that $R^+ = R^- = R^H$, when classical first-order Taylor expansion homogenization is employed, because the structure is symmetric with $\zeta_3^e = 0$. We first analyzed the apparent elements as they appear in Eq. (8) and as calculated numerically. The normalized values $\zeta_3^e c_0$ and $B_a^e/\gamma P_0$ are depicted in Figs. 2 (e,f) and Figs. 2 (g,h) for $(\theta, \psi) = (0, 0)$ and $(\theta, \psi) = (\frac{\pi}{3}, \frac{\pi}{6})$ respectively. Figure 2 (b) depicts the normalized density ρ_3^e/ρ_0, which does not depend on the angle of incidence. The dependence of both ζ_3^e and B_a^e on $\mathbf{k}_\perp$ is clearly visible. The effective and apparent properties directly calculated from Eqs. (8, 9) are in excellent agreement with those numerically calculated, thus validating the theoretical expressions. We also numerically verify that $\zeta_{3,num}^e = -\xi_{3,num}^e$. While the imaginary part of $\zeta_3^e c_0$ vanishes at low frequency, its real part goes to a finite value because of the viscous regime of the porous materials, i.e., $\rho_i^{(j)}/\rho_0 \approx \frac{\alpha_i^{(j)}}{\phi^{(j)}} + \mathbf{i}\frac{\eta/K_i}{\omega\rho_0}$, $i = \parallel, \perp$, and $j = 1, 2$. This prevents the opening of a band gap at low frequency, which could have resulted from a purely imaginary value of ζ_3^e. Only ζ_3^e starts to deviate from $\zeta_{3,num}^e$ for frequencies higher than 400 Hz. This should be mitigated by the fact that the dispersion relation $k^e = \omega\sqrt{(\zeta_3^e)^2 + \rho^e/B_a^e}$ is correctly modeled by the effective properties as shown in Figs. 2 (i,j). Note that $\mathrm{Re}(k^e d)$ becomes larger than ≈ 0.2 for $f > 400$ Hz. The low frequency requirement is thus theoretically no longer satisfied in this frequency range. Both the properties and the scattering coefficients, depicted in Figs. 2 (c,d), seem to be correctly modeled even for much larger values of $\mathrm{Re}(k^e d)$, while it is usually accepted that low frequency approximation is valid for $\mathrm{Re}(k^e d) < 0.1$. For the sake of comparison, the reflection and transmission coefficients, R^H and T^H, calculated with $\zeta_3^a = 0$,

i.e., classical homogenization results, are plotted on Figs. 2 (c,d). Although the transmission coefficient is correctly modeled whatever the order of the Taylor expansion considered to derive the effective properties, the reflection coefficients become different for $f > 200$ Hz, which roughly corresponds to $\mathrm{Re}\,(k^e d) < 0.1$. The Willis coupling is thus a key parameter to model laminated structures, allowing to correctly account for the geometrical and material asymmetry. The frequency range of validity and accuracy of the effective properties is widened simply because a second-order instead of a first-order Taylor expansion is considered. This was already pointed out in Ref. [6] and is also partly due to the non-resonant feature of the present structure. The dispersion relations calculated in the absence of the Willis coupling, i.e., classical homogenization, are also plotted in Figs. 2 (i,j) and are found in good agreement with those numerically evaluated and calculated with the effective Willis coupling. Thus, this coupling mostly impacts the impedances $Z_a^{\pm} = B_a^e \left(\sqrt{\left(\zeta_3^e\right)^2 + \rho^e / B_a^e} \pm \zeta_3^e \right)$ translating the structural asymmetry into different reflection coefficients when the laminate is excited from the positive or the negative $\mathbf{x}_3$-directions.

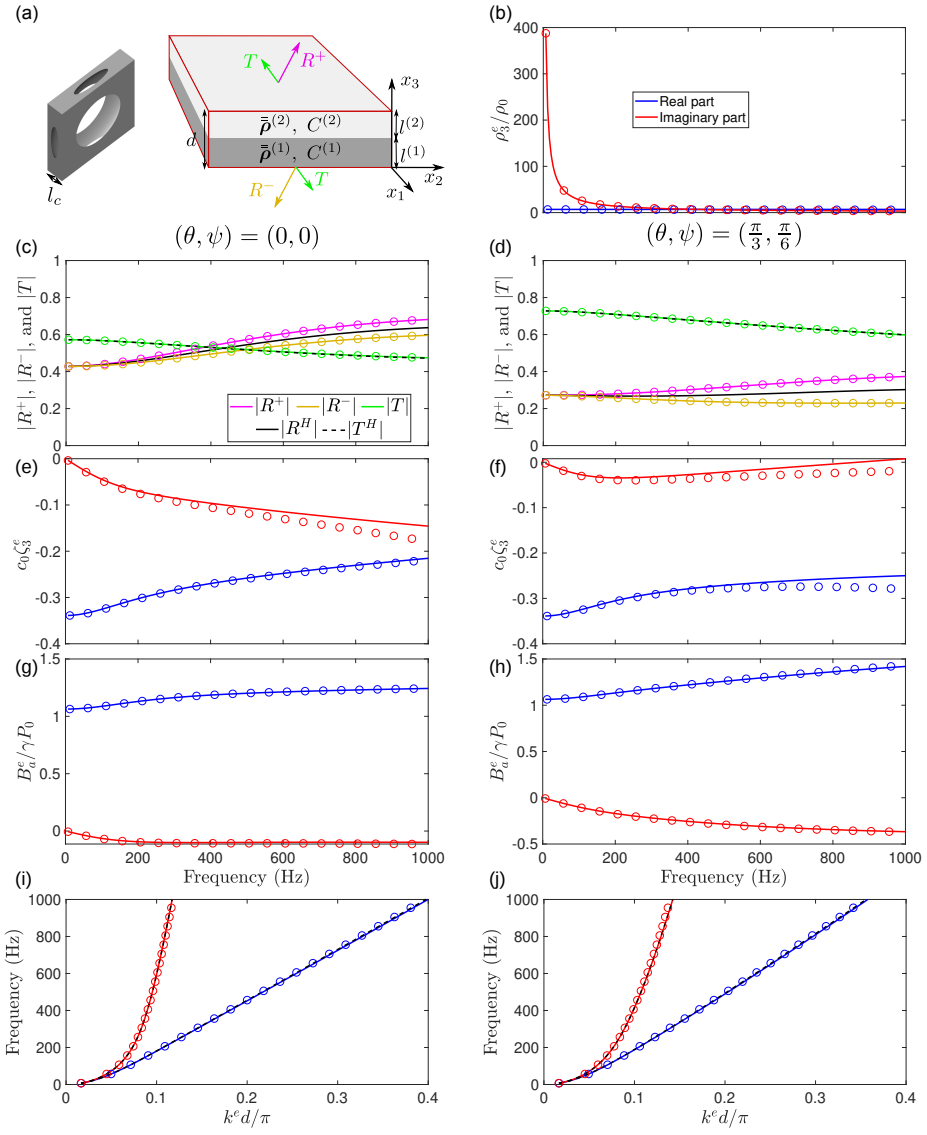

Figure 2: [Color online] Sketch of the laminate unit cell together with the micro-structure unit cell (a). Absolute value of the reflection and transmission coefficients (c-d) of a $L = d$-thick laminate ($N = 1$), normalized Willis coupling (e-f), normalized apparent bulk modulus (g-h), and dispersion relation -black lines depict the classical homogenization results- (i,j) for $(\theta, \psi) = (0, 0)$ and $(\theta, \psi) = (\frac{\pi}{3}, \frac{\pi}{6})$. The normalized density along the $\mathbf{x}_3$-direction is depicted in (b). Real (blue curves) and imaginary (red curves) parts of each element are depicted. Elements calculated with the effective parameters are plotted in solid line and those numerically evaluated are plotted with circle symbols.

To get a grip on the effective parameters, the normalized Willis coupling ζ_3^e, in-plane $\rho_\perp^e/\rho_0 = \rho_2^e/\rho_0 = \rho_1^e/\rho_0$ and out-of-plane $\rho_\parallel^e/\rho_0 = \rho_3^e/\rho_0$ normalized densities, and the normalized value of the bulk modulus $B^e/\gamma P_0$ are plotted Figs. 3 (a,b,c). To make it clearer and because the considered Willis material is orthotropic, the Willis coupling is decomposed into a local part and a nonlocal part as $\zeta_3^e = \zeta_3^{e,l} + (k_1/k_0)^2\zeta_3^{e,nl} + (k_2/k_0)^2\zeta_3^{e,nl}$. Obviously, this decomposition is not optimal, because $\zeta_3^{e,nl}$ then depends on the surrounding fluid properties. Nevertheless, the influence of $\zeta_3^{e,nl}$, notably at high frequency, is clearly visible. All Willis terms vanish at low frequency but the real part of the local Willis coupling because of the viscous regime. The orthotropy of the Willis material is clearly visible in Fig. 3 (b). For completeness, the reflection and transmission coefficients of a $L = 5d$-thick laminate calculated with the effective properties (both first- and second-order) and with the full transfer matrix are plotted in Fig. 3 (d) for $(\theta, \psi) = (\frac{\pi}{3}, \frac{\pi}{6})$. Again, the frequency range of validity and accuracy of the effective properties when the Willis coupling is accounted for is clearly evidenced.

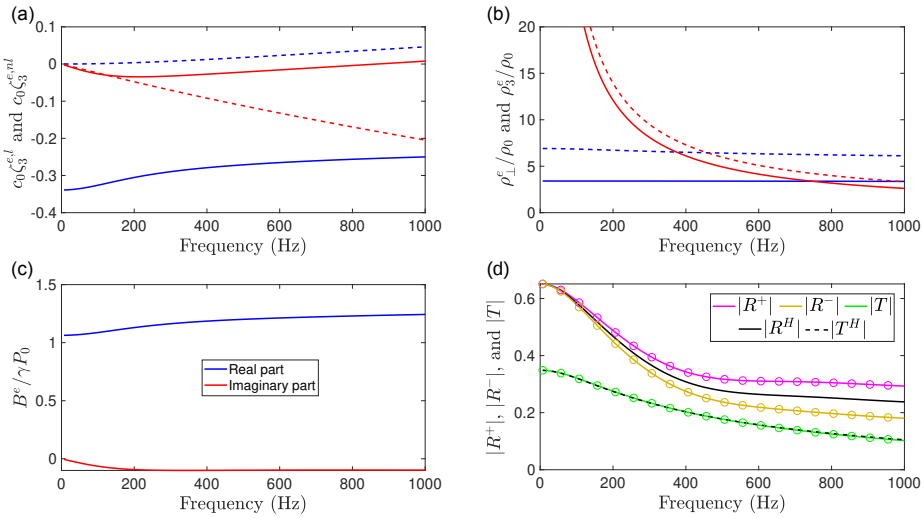

Figure 3: [Color Online] Normalized effective properties of the laminate porous material: local (solid line) and nonlocal (dashed line) Willis couplings (a), out-of-plane (dashed line) and in-plane (solid lines) densities (b), and bulk modulus (c). Real parts are plotted in blue lines and imaginay parts in red lines. The absolute values of the reflection and transmission coefficients of a $L = 5d$-thick laminate ($N = 5$) for $(\theta, \psi) = (\frac{\pi}{3}, \frac{\pi}{6})$ as calculated via Eqs. (8, 9, 10) and via the total transfer matrix (d). Coefficients calculated with the effective parameters are plotted in solid lines and the numerically evaluated elements are plotted with circle symbols.

5. General form of the effective properties of a laminate

To derive the general form of the effective properties of a laminate, we consider a laminated unit cell of thickness d composed of N layers of material $M^{(j)}$ of density tensor $\bar{\bar{\boldsymbol{\rho}}}^{(j)}$, compressiblity $C^{(j)}$, and thickness $l^{(j)}$, $j \in \mathcal{N} = [1, N]$, such that $d = \sum_{j\in\mathcal{N}} l^{(j)}$. Following the procedure described in Section 2.2, we

end with

$$\rho_3^e = \sum_{j\in\mathcal{N}} \rho_3^{(j)} \frac{l^{(j)}}{d},\ \frac{1}{\rho_1^e} = \sum_{j\in\mathcal{N}} \frac{l^{(j)}}{d\rho_1^{(j)}},\ \frac{1}{\rho_2^e} = \sum_{j\in\mathcal{N}} \frac{l^{(j)}}{d\rho_2^{(j)}},\ C^e = \sum_{j\in[1,N]} C^{(j)} \frac{l^{(j)}}{d}\ ,$$
$$\xi_1^e = -\zeta_1^e = 0,\ \xi_2^e = -\zeta_2^e = 0,$$
$$\zeta_3^e = -\xi_3^e = \sum_{j\in\mathcal{N}} \sum_{i>j} \frac{-\mathrm{i}\omega l^{(j)} l^{(i)}}{2d} \left(\rho_3^{(j)} C_a^{(i)} - \rho_3^{(i)} C_a^{(j)}\right)$$
$$= \sum_{j\in\mathcal{N}} \sum_{i>j} \frac{-\mathrm{i}\omega l^{(j)} l^{(i)}}{2d} \left(\rho_3^{(j)} C^{(i)} - \rho_3^{(i)} C^{(j)} + \frac{(k_1)^2}{\omega^2} \left(\frac{\rho_3^{(i)}}{\rho_1^{(j)}} - \frac{\rho_3^{(j)}}{\rho_1^{(i)}}\right) + \frac{(k_2)^2}{\omega^2} \left(\frac{\rho_3^{(i)}}{\rho_2^{(j)}} - \frac{\rho_3^{(j)}}{\rho_2^{(i)}}\right)\right). \tag{14}$$

Note that the derivation of these general formulae are straigthfoward via the Padé approximation and seems more complex via the Baker–Campbell–Hausdorff formula [23].

6. Conclusion

The closed forms of the effective properties of an anisotropic two-material fluid laminate are derived thanks to the Padé approximation of the total transfer matrix. These closed forms rely on second-order Taylor expansions of the transfer matrix elements, allowing the derivation of the Willis coupling. This Willis coupling is composed of a purely local term and nonlocal terms that depend on the projection of the wavenumber on the in-plane directions. The nonlocality directly impacts the governing equations modeling the acoustic wave propagation in these Willis materials, which then involve convolution products in space. This highlights the dependence of the Willis coupling on the in-plane coordinates and thus on the angle of incidence, suggesting that the form of the governing equations, although providing the accurate propagation matrix, could be inadequate to describe the three-dimensional acoustic wave propagation in fluid laminates. The nonlocal Willis coupling arises from the apparent compressibility. While the effective density and bulk modulus are weighted sum of the material properties that compose the laminate, the Willis coupling involves their difference. Thus, the derived closed form requires orientating the laminate, which is the reason why the nonlocal Willis coupling is even in our formulation.

In practice, the Willis coupling widens the frequency range of validity and accuracy of the effective properties and thus of the calculated scattering coefficients when compared to classical homogenization results for which the Willis coupling is absent. This widening is mostly attributed to a better modeling of the material impedance thanks to the Willis coupling. As an example, a two-orthotropic porous material laminate is considered. All effective properties and scattering coefficients are found in good agreements. The general forms of the effective properties of a laminate are provided. Beyond easing the engineering use of Willis materials, this article also aims at providing the basis of the experimental characterization of 2 or 3 dimensional planar Willis materials by inverting the propagation matrix derived in the present article.

Acknowledgments

J.-P.G., M.M., T.C. and V.R.-G. would like to acknowledge the support of the ANR-RGC METARoom project (ANR-18-CE08-0021). J.L. would like to acknowledge the support of the Research Grants Council in Hong Kong (Grant No. 16302218). D.T. acknowledges financial support through the "Ramón y Cajal" fellowship under grant number RYC-2016-21188.

Appendix A. Derivation of the propagation matrix

The system Eqs.(1) is first expanded as

$$\begin{aligned}
&\mathrm{i}\omega\xi_1 p + \mathrm{i}\omega\rho_1 V_1 = \frac{\partial p}{\partial x_1} \ , \\
&\mathrm{i}\omega\xi_2 p + \mathrm{i}\omega\rho_2 V_2 = \frac{\partial p}{\partial x_2} \ , \\
&\mathrm{i}\omega\xi_3 p + \mathrm{i}\omega\rho_3 V_3 = \frac{\partial p}{\partial x_3} \ , \\
&\mathrm{i}\omega\zeta_1 V_1 + \mathrm{i}\omega\zeta_2 V_2 + \mathrm{i}\omega\zeta_3 V_3 + \mathrm{i}\omega C p = \frac{\partial V_1}{\partial x_1} + \frac{\partial V_2}{\partial x_2} + \frac{\partial V_3}{\partial x_3} \ .
\end{aligned} \tag{A.1}$$

Introducing $\tilde{a}(k_1, k_2, x_3)$ the in-plane spatial Fourrier transform of $a(\mathbf{x})$, such that $a = \iint_{-\infty}^{\infty} \tilde{a} e^{\mathrm{i}k_1 x_1 + \mathrm{i}k_2 x_2} dx_1 dx_2$, the in-plane spatial Fourrier transform of

Eqs.(A.1) reads as

$$\begin{aligned}
&\mathrm{i}\omega\xi_1\tilde{p} + \mathrm{i}\omega\rho_1\tilde{V}_1 = \mathrm{i}k_1\tilde{p} \ , \\
&\mathrm{i}\omega\xi_2\tilde{p} + \mathrm{i}\omega\rho_2\tilde{V}_2 = \mathrm{i}k_2\tilde{p} \ , \\
&\mathrm{i}\omega\xi_3\tilde{p} + \mathrm{i}\omega\rho_3\tilde{V}_3 = \frac{\partial\tilde{p}}{\partial x_3} \ , \\
&\mathrm{i}\omega\zeta_1 V_1 + \mathrm{i}\omega\zeta_2 V_2 + \mathrm{i}\omega\zeta_3\tilde{V}_3 + \mathrm{i}\omega C\tilde{p} = \mathrm{i}k_1\tilde{V}_1 + \mathrm{i}k_2\tilde{V}_2 + \frac{\partial\tilde{V}_3}{\partial x_3} \ .
\end{aligned} \tag{A.2}$$

From the first two equations, it is clear that $\tilde{V}_1 = (k_1 - \omega\xi_1)\,\tilde{p}/\omega\rho_1$ and $\tilde{V}_2 = (k_2 - \omega\xi_2)\,\tilde{p}/\omega\rho_2$. The introduction of these expressions in the fourth equation leads, together with the third equation, to the following first order differential system

$$\begin{aligned}
\frac{\partial\tilde{p}}{\partial x_3} &= \mathrm{i}\omega\xi_3\tilde{p} + \mathrm{i}\omega\rho_3\tilde{V}_3 \ , \\
\frac{\partial\tilde{V}_3}{\partial x_3} &= \mathrm{i}\omega C\tilde{p} + \mathrm{i}\,(\omega\zeta_1 - k_1)\,\tilde{V}_1 + \mathrm{i}\,(\omega\zeta_2 - k_2)\,\tilde{V}_2 + \mathrm{i}\omega\zeta_3\tilde{V}_3 \\
&= \left[\mathrm{i}\omega C - \frac{\mathrm{i}\,(k_1 - \omega\zeta_1)\,(k_1 - \omega\xi_1)}{\omega\rho_1} - \frac{\mathrm{i}\,(k_2 - \omega\zeta_2)\,(k_2 - \omega\xi_2)}{\omega\rho_2}\right]\tilde{p} + \mathrm{i}\omega\zeta_3\tilde{V}_3 \ ,
\end{aligned} \tag{A.3}$$

which can then be cast in the form of Eqs. (2) and (3).

Appendix B. Derivation of the effective properties from the total transfer matrix of a two-fluid laminate

The total transfer matrix of the two-fluid laminate unit cell is

$$\mathbf{T}_d = \mathbf{T}_{l^{(2)}}\mathbf{T}_{l^{(1)}} = \begin{bmatrix} c^{(1)}c^{(2)} - \dfrac{s^{(1)}s^{(2)}Z_a^{(2)}}{Z_a^{(1)}} & \mathrm{i}Z_a^{(1)}s^{(1)}c^{(2)} + \mathrm{i}Z_a^{(2)}s^{(2)}c^{(1)} \\ \dfrac{\mathrm{i}c^{(1)}s^{(2)}}{Z_a^{(2)}} + fracic^{(2)}s^{(1)}Z_a^{(1)} & c^{(1)}c^{(2)} - \dfrac{s^{(1)}s^{(2)}Z_a^{(1)}}{Z_a^{(2)}} \end{bmatrix}, \tag{B.1}$$

where $c^{(j)} = \cos\left(k_a^{(j)} l^{(j)}\right)$ and $s^{(j)} = \sin\left(k_a^{(j)} l^{(j)}\right)$, $j = 1, 2$. Second order expansion of each element t_{ij}, $(i, j) \in [1, 2]^2$ thus reads as

$$\begin{aligned}
t_{1,1} &= 1 - \frac{\left(k_a^{(1)} l^{(1)}\right)^2}{2} - \frac{\left(k_a^{(2)} l^{(2)}\right)^2}{2} - \frac{Z_a^{(2)} k_a^{(1)} l^{(1)} k_a^{(2)} l^{(2)}}{Z_a^{(1)}} + \mathcal{O}\left(kd\right)^3, \\
t_{1,2} &= \mathrm{i} Z_a^{(1)} k_a^{(1)} l^{(1)} + \mathrm{i} Z_a^{(2)} k_a^{(2)} l^{(2)} + \mathcal{O}\left(kd\right)^3, \\
t_{2,1} &= \frac{\mathrm{i} k_a^{(1)} l^{(1)}}{Z_a^{(1)}} + \frac{\mathrm{i} k_a^{(2)} l^{(2)}}{Z_a^{(2)}} + \mathcal{O}\left(kd\right)^3, \\
t_{2,2} &= 1 - \frac{\left(k_a^{(1)} l^{(1)}\right)^2}{2} - \frac{\left(k_a^{(2)} l^{(2)}\right)^2}{2} - \frac{Z_a^{(1)} k_a^{(1)} l^{(1)} k_a^{(2)} l^{(2)}}{Z_a^{(2)}} + \mathcal{O}\left(kd\right)^3,
\end{aligned} \tag{B.2}$$

which leads to

$$\begin{aligned}
a_{1,1} &= \frac{2\left(t_{1,1} - t_{2,2}\right)}{d\left(2 + t_{1,1} + t_{2,2}\right)} = \frac{k_a^{(1)} l^{(1)} k_a^{(2)} l^{(2)}}{2d} \left(\frac{Z_a^{(1)}}{Z_a^{(2)}} - \frac{Z_a^{(2)}}{Z_a^{(1)}}\right) + O\left(kd\right)^3, \\
a_{1,2} &= \frac{4 t_{1,2}}{d\left(2 + t_{1,1} + t_{2,2}\right)} = \frac{\mathrm{i}\left(Z_a^{(1)} k_a^{(1)} l^{(1)} + Z_a^{(2)} k_a^{(2)} l^{(2)}\right)}{d} + O\left(kd\right)^3, \\
a_{2,1} &= \frac{4 t_{2,1}}{d\left(2 + t_{1,1} + t_{2,2}\right)} = \frac{\mathrm{i}}{d} \left(\frac{k_a^{(1)} l^{(1)}}{Z_a^{(1)}} + \frac{k_a^{(2)} l^{(2)}}{Z_a^{(2)}}\right) + O\left(kd\right)^3, \\
a_{2,2} &= \frac{2\left(t_{2,2} - t_{1,1}\right)}{d\left(2 + t_{1,1} + t_{2,2}\right)} = \frac{k_a^{(1)} l^{(1)} k_a^{(2)} l^{(2)}}{2d} \left(\frac{Z_a^{(2)}}{Z_a^{(1)}} - \frac{Z_a^{(1)}}{Z_a^{(2)}}\right) + O\left(kd\right)^3.
\end{aligned} \tag{B.3}$$

Keeping in mind that $Z_a^{(j)} k_a^{(j)} = \omega \rho_3^{(j)}$ and $k_a^{(j)} / Z_a^{(j)} = \omega C_a^{(j)}$, we end up with Eqs. (8).

Appendix C. Derivation of the effective properties using the Baker–Campbell–Hausdorff formula

Inspired by [23], we derive the effective properties of a two-material fluid laminate by the Baker–Campbell–Hausdorff formula [24] in order to valid our analytical results. The Baker–Campbell–Hausdorff formula perfectly fits our problem, because the total transfer matrix reads as a multiplication of matrix exponentials. The story is completely different if the configuration incorporates point resonators whose transfer matrix does not take the form of a matrix

exponential [22]. The Baker–Campbell–Hausdorff formula is concerned with

$$\mathbf{exp}\left(\mathbf{Z}\right) = \mathbf{exp}\left(\mathbf{B}^{(1)}\right)\mathbf{exp}\left(\mathbf{B}^{(2)}\right), \tag{C.1}$$

where $\mathbf{B}^{(1)}$ and $\mathbf{B}^{(2)}$ are square matrices. The analytical expression of $\mathbf{Z} = \mathbf{log}\left(\mathbf{exp}\left(\mathbf{B}^{(1)}\right)\mathbf{exp}\left(\mathbf{B}^{(2)}\right)\right)$ is approximated at the first-order by

$$\mathbf{Z} \approx \mathbf{B}^{(1)} + \mathbf{B}^{(2)} + \frac{1}{2}\left[\mathbf{B}^{(1)}, \mathbf{B}^{(2)}\right], \tag{C.2}$$

where $\left[\mathbf{B}^{(1)}, \mathbf{B}^{(2)}\right] = \mathbf{B}^{(1)}\mathbf{B}^{(2)} - \mathbf{B}^{(2)}\mathbf{B}^{(1)}$ is the commutator of $\mathbf{B}^{(1)}$ and $\mathbf{B}^{(2)}$. Applying this formula to our problem, i.e., Eq. (6)

$$\mathbf{T}_d = \mathbf{exp}\left(\mathbf{A}^e d\right) = \mathbf{T}_{l^{(2)}}\mathbf{T}_{l^{(1)}} = \mathbf{exp}\left(\mathbf{A}^{(2)} l^{(2)}\right)\mathbf{exp}\left(\mathbf{A}^{(1)} l^{(1)}\right), \tag{C.3}$$

directly provides

$$\mathbf{A}^e = \begin{bmatrix} \dfrac{\omega^2 l^{(1)} l^{(2)}}{2d}\left(C_a^{(2)}\rho_3^{(1)} - C_a^{(1)}\rho_3^{(2)}\right) & \mathrm{i}\omega\dfrac{\rho_3^{(1)} l^{(1)} + \rho_3^{(2)} l^{(2)}}{d} \\ \mathrm{i}\omega\dfrac{C_a^{(1)} l^{(1)} + C_a^{(2)} l^{(2)}}{d} & \dfrac{-\omega^2 l^{(1)} l^{(2)}}{2d}\left(C_a^{(2)}\rho_3^{(1)} - C_a^{(1)}\rho_3^{(2)}\right) \end{bmatrix}, \tag{C.4}$$

which are identical to the expressions provided in Eq. (8).

Appendix D. Rewritting the constitutive equations when the Willis parameters depend on $\mathbf{x}_\perp$

From Eqs. (9) and (10), it is clear that C_e and $\bar{\bar{\rho}}_e$ do not depend on $\mathbf{k}_\perp$, but that $\zeta_3^e(\mathbf{k}_\perp)$ and thus $\bar{\boldsymbol{\zeta}}^e(\mathbf{k}_\perp) = -\bar{\boldsymbol{\xi}}^e(\mathbf{k}_\perp) =< 0, 0, \zeta_3^e(\mathbf{k}_\perp) >^T$ do. Therefore, the Willis coupling is an in-plane spatial Fourier transform and should be $\tilde{\bar{\boldsymbol{\zeta}}}^e$ rather than $\bar{\boldsymbol{\zeta}}^e$. Each step of the derivation of the propagation matrix from the governing equations (detailed in Appendix A) is the same and can thus be followed in reverse, but the inverse spatial Fourier transform of the governing equations. Effectively, the system Eq. (A.2) becomes

$$\begin{aligned} &\mathrm{i}\omega\rho_1\tilde{V}_1 = \mathrm{i}k_1\tilde{p}\ , \\ &\mathrm{i}\omega\rho_2\tilde{V}_2 = \mathrm{i}k_2\tilde{p}\ , \\ &-\mathrm{i}\omega\tilde{\zeta}_3\tilde{p} + \mathrm{i}\omega\rho_3\tilde{V}_3 = \frac{\partial\tilde{p}}{\partial x_3}\ , \\ &\mathrm{i}\omega\tilde{\zeta}_3\tilde{V}_3 + \mathrm{i}\omega C\tilde{p} = \mathrm{i}k_1\tilde{V}_1 + \mathrm{i}k_2\tilde{V}_2 + \frac{\partial\tilde{V}_3}{\partial x_3}\ , \end{aligned} \tag{D.1}$$

the inverse spatial Fourier transform of which is

$$\begin{aligned}
&\mathrm{i}\omega\rho_1 V_1(\mathbf{x}) = \frac{\partial p(\mathbf{x})}{\partial x_1} \ , \\
&\mathrm{i}\omega\rho_2 \tilde{V}_2(\mathbf{x}) = \frac{\partial p(\mathbf{x})}{\partial x_2} \ , \\
&-\mathrm{i}\omega\zeta_3(\mathbf{x}_\perp) \star_\perp p(\mathbf{x}) + \mathrm{i}\omega\rho_3\tilde{V}_3 = \frac{\partial \tilde{p}(\mathbf{x})}{\partial x_3} \ , \\
&\mathrm{i}\omega\zeta_3(\mathbf{x}_\perp) \star_\perp \tilde{V}_3(\mathbf{x}) + \mathrm{i}\omega C p(\mathbf{x}) = \frac{\partial V_1(\mathbf{x})}{\partial x_1} + \frac{\partial V_2(\mathbf{x})}{\partial x_2} + \frac{\partial V_3}{\partial x_3} \ ,
\end{aligned} \tag{D.2}$$

where the spatial dependence has been highlighted, $\zeta_3(\mathbf{x}_\perp) = \iint_{-\infty}^{\infty} \tilde{\zeta}_3(\mathbf{k}_\perp) e^{\mathrm{i}\mathbf{k}_\perp\cdot\mathbf{x}_\perp} d\mathbf{x}_\perp/4\pi^2$, and $\star_\perp$ is a convolution product along the in-plane component $\mathbf{x}_\perp$. This system can thus be cast in the form of Eq. (11).

References

[1] J. Willis, Variational principles for dynamic problems for inhomogeneous elastic media, Wave Motion 3 (1981) 1 – 11.

[2] I. Lindell, A. Sihvola, S. Tretyakov, A. J. Viitanen, Electromagnetic waves in chiral and bi-isotropic media, Artech House, 1994, pp. 1–22.

[3] S. Koo, C. Cho, J. Jeong, N. Park, Acoustic omni meta-atom for decoupled access to all octants of a wave parameter space, Nat Commun 7 (2016) 13012.

[4] M. B. Muhlestein, C. F. Sieck, P. S. Wilson, M. R. Haberman, Experimental evidence of willis coupling in a one-dimensional effective material element, Nat Commun 8 (2017) 15625.

[5] Y. Liu, Z. Liang, J. Zhu, L. Xia, O. Mondain-Monval, T. Brunet, A. Alù, J. Li, Willis metamaterial on a structured beam, Phys. Rev. X 9 (2019) 011040.

[6] C. F. Sieck, A. Alù, M. R. Haberman, Origins of willis coupling and acoustic bianisotropy in acoustic metamaterials through source-driven homogenization, Phys. Rev. B 96 (2017) 104303.

[7] M.-F. Ponge, P. O., D. Torrent, Dynamic homogenization theory for non-local acoustic metamaterials, Extreme Mechanics Letters 12 (2017) 71 – 76.

[8] A. L. Shuvalov, A. A. Kutsenko, A. N. Norris, O. Poncelet, Effective willis constitutive equations for periodically stratified anisotropic elastic media, Proc. R. Soc. A. 467 (2011) 1749–1769.

[9] S. Nemat-Nasser, J. R. Willis, A. Srivastava, A. V. Amirkhizi, Homogenization of periodic elastic composites and locally resonant sonic materials, Phys. Rev. B 83 (2011) 104103.

[10] A. Melnikov, Y. K. Chiang, Q. Li, S. Oberst, A. Alù, S. Marburg, D. Powell, Acoustic meta-atom with experimentally verified maximum willis coupling, Nat Commun 10 (2019) 3148.

[11] H. Nassar, X. Xu, A. Norris, G. Huang, Modulated phononic crystals: Non-reciprocal wave propagation and willis materials, J. Mech. Phys. Solids 101 (2017) 10–29.

[12] L. Quan, D. L. Sounas, A. Alù, Nonreciprocal willis coupling in zero-index moving media, Phys. Rev. Lett. 123 (2019) 064301.

[13] Y. Zhai, H.-S. Kwon, B.-I. Popa, Active willis metamaterials for ultra-compact nonreciprocal linear acoustic devices, Phys. Rev. B 99 (2019) 220301(R).

[14] C. Cho, X. Wen, N. Park, J. Li, Acoustic willis meta-atom beyond the bounds of passivity and reciprocity, Commun. Phys. 4 (2021) 82.

[15] C. Olivier, G. Poignand, M. Malléjac, V. Romero-García, G. Penelet, A. Merkel, D. Torrent, J. Li, J. Christensen, J.-P. Groby, Nonreciprocal and even willis couplings in periodic thermoacoustic amplifiers, Phys. Rev. B 104 (2021) 184109.

[16] L. Landau, E. Lifshitz, Chapter XII - spatial dispersion, in: L. Landau, E. Lifshitz (Eds.), Electrodynamics of Continuous Media (Second Edition), second edition Edition, Vol. 8 of Course of Theoretical Physics, Pergamon, Amsterdam, 1984, pp. 358–371.

[17] N. Nemati, A. Kumar, D. Lafarge, N. Fang, Nonlocal description of sound propagation through an array of helmholt z resonators, Comptes Rendus Mécanique 343 (12) (2015) 656–669.

[18] N. Nemati, Y. E. Lee, D. Lafarge, A. Duclos, N. Fang, Nonlocal dynamics of dissipative phononic fluids, Phys. Rev. B 95 (2017) 224304.

[19] L. Quan, A. Alù, Passive acoustic metasurface with unitary reflection based on nonlocality, Phys. Rev. Applied 11 (2019) 054077.

[20] N. Geib, A. Sasmal, Z. Wang, Y. Zhai, B.-I. Popa, K. Grosh, Tunable nonlocal purely active nonreciprocal acoustic media, Phys. Rev. B 103 (2021) 165427.

[21] D. Lafarge, Acoustic Waves in Periodic Structures, Metamaterials, and Porous Media, Springer International Publishing, Cham., 2021, Ch. Nonlocal Dynamic Homogenization of Fluid-Saturated Metamaterials, pp. 273–331.

[22] J.-P. Groby, M. Malléjac, A. Merkel, V. Romero-García, V. Tournat, D. Torrent, J. Li, Analytical modeling of one-dimensional resonant asymmetric and reciprocal acoustic structures as willis materials, New J. Phys. 23 (2021) 053020.

[23] Y. Liu, S. Guenneau, B. Gralak, Artificial dispersion via high-order homogenization: magnetoelectric coupling and magnetism from dielectric layers, Proc. R. Soc. A: Math. Phys. Eng. Sci. 469 (2013) 20130240.

[24] G. H. Weiss, A. A. Maradudin, The baker-hausdorff formula and a problem in crystal physics, J. Math. Phys. 3 (1962) 771–777.

[25] O. Tanneau, J. B. Casimir, P. Lamary, Optimization of multilayered panels with poroelastic components for an acoustical transmission objective, J. Acoust. Soc. Am. 120 (2006) 1227–1238.

[26] J. Boulvert, T. Cavalieri, J. Costa-Baptista, L. Schwan, V. Romero-García, G. Gabard, E. R. Fotsing, A. Ross, J. Mardjono, J.-P. Groby, Optimally graded porous material for broadband perfect absorption of sound, J. Appl. Phys. 126 (2019) 175101.

[27] T. Cavalieri, J. Boulvert, G. Gabard, V. Romero-García, M. Escouflaire, J. Regnard, J.-P. Groby, Graded and anisotropic porous materials for broadband and angular maximal acoustic absorption, Materials 13 (2020).

[28] A. Terroir, L. Schwan, T. Cavalieri, V. Romero-García, G. Gabard, J.-P. Groby, General method to retrieve all effective acoustic properties of fully-anisotropic fluid materials in three dimensional space, J. Appl. Phys. 125 (2019) 025114.

[29] N. Jiménez, J.-P. Groby, V. Romero-García, Acoustic Waves in Periodic Structures, Metamaterials, and Porous Media, Springer International Publishing, Cham., 2021, Ch. The Transfer Matrix Method in Acoustics, pp. 103–164.

[30] B. Brouard, D. Lafarge, J.-F. Allard, A general method of modelling sound propagation in layered media, Journal of Sound and Vibration 183 (1995) 129–142.

[31] J.-L. Auriault, C. Boutin, C. Geindreau, Homogenization of Coupled Phenomena in Heterogenous Media, John Wiley & Sons, London, UK; Hoboken, NJ, USA, 2009.

[32] D. L. Johnson, J. Koplik, R. Dashen, Theory of dynamic permeability and tortuosity in fluid-saturated porous media, J. Fluid Mech. 176 (1987) 379–402.

[33] D. Lafarge, P. Lemarinier, J.-F. Allard, V. Tarnow, Dynamic compressibility of air in porous structures at audible frequencies, J. Acoust. Soc. Am. 102 (1997) 1995–2006.